Article

Not peer-reviewed version

The Influence of Free Movement in the Opposite Direction to the Obstacle on the Dynamics and Efficiency of a Single-Sided Vibro-Impact Nonlinear Energy Sink

Petro Lizunov , Olga Pogorelova , Tetyana Postnikova *

Posted Date: 1 April 2026

doi: 10.20944/preprints202604.0099.v1

Keywords: vibro-impact; damper; nonlinear energy sink; tuned mass damper; mitigating vibrations; optimization; away from the obstacle

 doi:10.20944/preprints202604.0099.v1

Article

The Influence of Free Movement in the Opposite Direction to the Obstacle on the Dynamics and Efficiency of a Single-Sided Vibro-Impact Nonlinear Energy Sink

Petro Lizunov [1], Olga Pogorelova [2] and Tetyana Postnikova [2,*]

[1] Department of Structural Mechanics, Kyiv National University of Construction and Architecture, 31 Povitryanykh Syl Ave., Kyiv, Ukraine, 03680

[2] Research Institute of Structural Mechanics, Kyiv National University of Construction and Architecture, 31 Povitryanykh Syl Ave., Kyiv, Ukraine, 03680

* Correspondence: posttan@ukr.net

Featured Application

The study of the performance and efficiency of vibro-impact nonlinear energy sinks in mitigating vibrations of the main structure conducted in this work allows us to understand and evaluate their optimal characteristics and operation, which will help to select advantageous designs for future applications.

Abstract

This paper studies the effect of the movement of a single-sided vibro-impact nonlinear energy sink (SSVI NES) in the direction opposite to the obstacle on its dynamics and efficiency in mitigating vibrations of the primary structure (PS) subjected to the harmonic excitation. The damper efficiency is assessed by the reduction of PS maximum mechanical energy. All damper parameters are optimized simultaneously. The paper focuses on the SSVI NES with free movement in the direction opposite to the obstacle, without any constraints, which ensures its high efficiency. Its dynamics and efficiency are compared with those of other dampers, namely SSVI NES with limited motion away from the obstacle and the tuned mass damper (TMD). The preservation of damper tuning when changing the structural parameters such as the natural frequency of the PS, its damping and the intensity of the harmonic exciting force is also being studied. The dynamics of SSVI NES with free motion away from the obstacle is quite calm with periodic motion over almost the entire frequency range. Rapid alternation of modes with different periodicity and different numbers of impacts per cycle, as well as irregular modes, is observed only at high frequencies of the exciting force.

Keywords: vibro-impact; damper; nonlinear energy sink; tuned mass damper; mitigating vibrations; optimization; away from the obstacle

1. Introduction

For a long time, the problem of mitigating vibrations in the main structure challenged the engineers and scientists. Among its various solutions, the passive vibration control has proven to be a fairy effective, robust and inexpensive method. Passive vibration control devices with linear coupling to the main structure have become known as the tuned mass dampers (TMDs). Their performance and efficiency have been studied in numerous works [1–4]. They found application in engineering practice and were used in a number of famous structures [5]. Two decades ago, the theory of Targeted Energy Transfer (TET) was proposed and published. Within the framework of this theory, the passive vibration control devices with nonlinear coupling to the main structure began to

 doi:10.20944/preprints202604.0099.v1

be actively discussed; they began to be called nonlinear energy sinks (NESs). During this time, NESs of different designs have been introduced [6–13]. Different types of NESs have been studied continuously to accommodate various engineering requirements [14]. In this paper, the authors provide a brief list of proposed NES types and accompany it with relevant references. They point out the high sensitivity of NESs to changes in the external excitation intensity, which limits their implementation in practical applications, since the amplitude of external excitation significantly influences the robustness of NESs. The proposed a stable state adjustable NES structure provides a new NES configuration that realizes the vibration reduction mechanism, which can effectively suppress the vibration under different excitation intensities. In the paper [15], the authors note that to trigger a TET, a sufficiently high initial energy and NES mass are required. New combining structures were proposed to overcome the problem of large additional mass and enhance vibration suppression performance. In [15], the combination of a cubic NES with a fractional-order inerter is studied. The study [16] introduces a novel vibration suppression system combining a TMD with an inerter and a vibro-impact NES in a parallel configuration. In [17], the system of the parallel NES cells coupled to the primary structure (PS) is proposed. It has been shown that, under harmonic excitation, increasing both the number of NES cells and the mass ratio significantly enhances the energy absorption performance of the system.

The study [18] investigates the mechanisms of vibration suppression and energy harvesting of a piezoelectric bistable NES coupled with multi-degree-of-freedom primary structures (in particular, with two-degree-of-freedom) and provides practical guidance for selecting parameters such as stiffness, mass, and damping in real-world engineering applications.

Many authors [19,20] believe that NES is an effective alternative to TMD, overcoming many of its limitations, one of which is the narrow operational frequency range. The NES with nonlinear connection to the PS employs a nonlinear restoring force, which allows it to resonate across multiple frequencies and provides a much broader operational frequency bandwidth [19].

One of the effective NES types is considered to be a vibro-impact NES (VI NES), in particular a single-sided VI NES (SSVI NES) [21,22]. The authors of TET theory presented a comprehensive paper [23], in which they provided a brief overview of vibration absorbers. They pointed out some of the shortcomings of TMDs, in particular, the possibility of efficient TET from the host structure into the TMD in a narrow frequency range and the detuning effect when the critical natural frequency of the host structure is shifted. They noted that using VI NESs for vibration mitigation is not merely a purely academic concept. They have the potential to be used in active industrial research, for example, in the development of aircraft turbine blades. In this paper, the authors study applying VI NESs to rotationally periodic host structures. Different dynamic regimes of the system were studied both analytically and numerically, and their effect on vibration mitigation was examined.

The energy transfer mechanism is comprehensively investigated in [24]. The vibration damping performance of the VI NES for the beam under harmonic force, broadband white noise, and transient shock excitations are also discussed in this paper and compared to other types of absorbers, namely TMD and cubic NES. The authors believe that due to the unique mechanism of VI NES, it can realize effective targeted energy transfers not only between the main structure and the VI NES, but also among the linear modes of the main structure itself. The parameter optimization showed that the main parameters that affect the vibration suppression performance of the VI NES are the clearance and the damper location on the beam, but not the vibro-impact damping.

The advantage of a soft vibro-impact interface is discussed in [6,20,25]. Comparison of the VI NES with the softened and hard contact is made in [6]. The authors in [20] explore various options for generating restoring force in NES. They consider a hardening and a softening NES, as well as NES with a periodically extended stiffness characteristic. They state that this stiffness results in an NES with a wider energy bandwidth than the conventional NES for harmonic excitations. However, they point out that despite these promising findings, the practical realization of the softening NES remains an open challenge. In [25], a soft vibro-impact interface, that is, materials with a lower Young's modulus, is proposed for passive vibration suppression. This work offers a combined theoretical–

 doi:10.20944/preprints202604.0099.v1

experimental investigation of a cantilever-based impact damper using a viscoelastic silicone rubber interface. The contact force during a soft impact is modeled as the sum of a linear elastic force and velocity-proportional damping.

Nevertheless, despite the appeal of NES, TMDs are widely used due to their simplicity and robustness and continue to be discussed in scientific literature, especially their application in combination with NES [26,27].

Design criterion of NES for the evaluation of vibration mitigation effect is discussed in [28]. The mechanical energy and the input energy of the main system, as well as displacement amplitude are suggested in as reasonable performance measures for evaluating the vibration mitigation effect of NES coupled with main system. It is worth noting that in this paper, the authors point out that all NES parameters must be optimized simultaneously to achieve the better mitigation effect.

In most works on SSVI NES, damper movement in the direction opposite to the obstacle is not considered. However, possible restrictions on this movement, or the lack thereof, significantly affect the performance of the system with SSVI NES coupled to the PS. There are four variants of this design, which are shown in Section 2. In this paper, we will focus on the performance of a system in which the SSVI NES moves freely away from the obstacle without any constraints, and compare it with the performance of the system in which this movement was limited by the presence of the PS itself. The dynamics and efficiency of a system with this design have been discussed in detail in several of our previous works [29,30].

2. SSVI NES Models with Different Designs

Four models of SSVI NESs with different designs (Figure 1) providing the various variants of damper movement in direction opposite to the obstacle can be considered. The obstacle is rigidly connected to the PS. The PS is the linear oscillator with k_1 stiffness and c_1 damping. The exciting force is harmonic $F(t) = Pcos\omega t$, its period is $T = 2\pi/\omega$.

The movement of the SSVI NES in the model in Figure 1a in the direction opposite to the obstacle is limited by the presence of PS itself. Therefore, the damper hits not only the obstacle, but also the PS directly. The impacts on the PS occur when the displacements of the bodies are equal $x_1 = x_2$, and on an obstacle when $x_2 = x_1 + D + C$. Thus, the SSVI NES of this model operates as an asymmetric double-sided VI NES striking obstacles on both sides. It is precisely this model that has been studied in detail in our previous works [29–31]. In this paper, this model will be used for comparison, where it will be referred to as SSbl NES (with bilateral impacts) for brevity.

Assuming that the damper design can prevent it from impacting the PS, we can consider the model shown in Figure 1b. The high stiffness of the connecting spring k_2 allows these impacts to ignore. Collision avoidance with PS imposes a constraint on the relationship between body displacements $x_1 < x_2$. Optimization procedures must be performed with this constraint in mind. The performance of this model was examined in detail in [32]. It was shown that this model hardly be considered successful in mitigating the PS vibrations. The model in Figure 1c also assumes no damper impacts on PS. It is similar to the model in Figure 1b, but the restriction is weaker $(x_1 - x_2) \leq L$; that is the impact is not allowed, but some displacements at a distance L are allowed. Finally, the SSVI NES in the model in Figure 1d moves freely, without any restrictions, in the direction opposite to the obstacle. It will be referred to as SSul NES (with unilateral impacts) for brevity in this paper. Its dynamics and efficiency are studied in this paper and compared with the performance of the SSVI NES in Figure 1a, i.e., SSbl NES, and TMD. It is worth noting that SSVI NES with unrestricted movement away from an obstacle was considered in [33,34].

 doi:10.20944/preprints202604.0099.v1

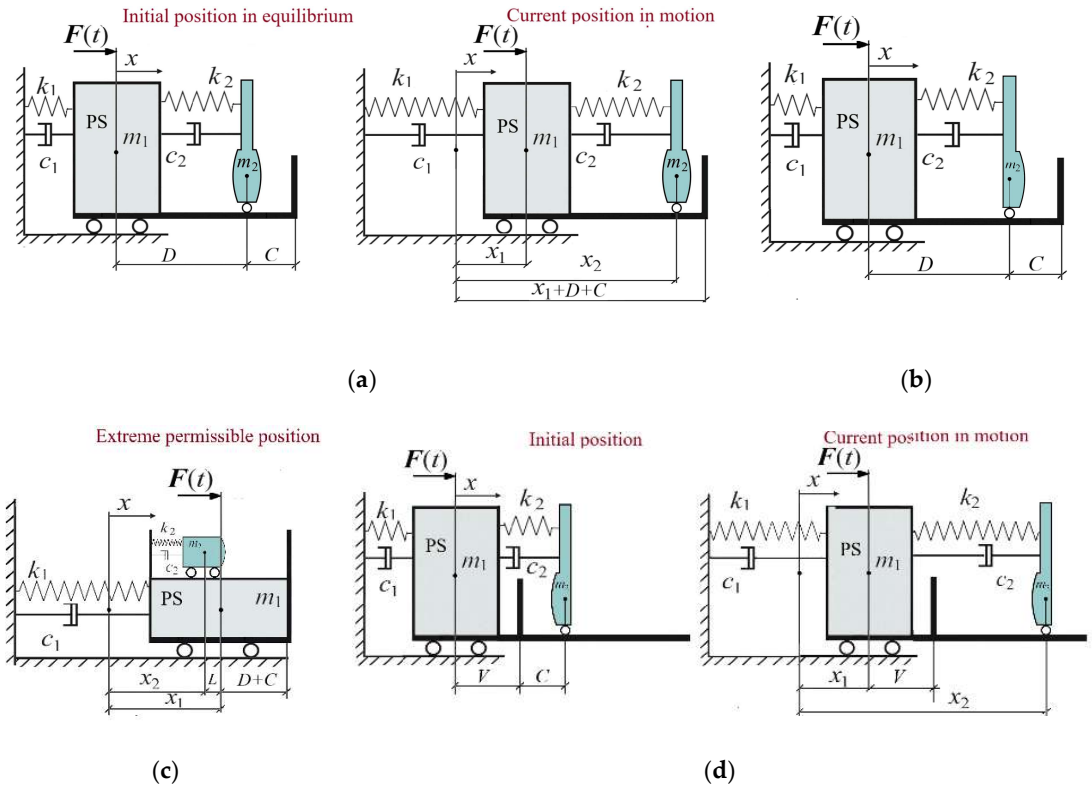

Figure 1. Conceptual schemes of a PS connected to a damper.

For the model of SSul NES shown in Figure 1d the Signorini's contact conditions are as follows:

$$x_2 \le (x_1 + V). \tag{1}$$

The contact impact force, which acts only during an impact, is simulated with the nonlinear Hertz's contact force according to his quasi-static contact theory [35]:

$$F_{con}(z) = K \cdot [z(t)]^{\frac{3}{2}}, \tag{2}$$

where $z(t)$ is the rapprochement of the colliding bodies during an impact due to the local body deformation allowed by the Hertz's contact theory

$$z = x_1 - x_2 + V. \tag{3}$$

Coefficient K characterizes the mechanical and geometrical properties of colliding surfaces:

$$K = \frac{4}{3}\frac{q_1}{(\delta_1+\delta_2)\sqrt{A+B}},\ \delta_1 = \frac{1-\nu_1^2}{E_1\pi},\ \delta_2 = \frac{1-\nu_2^2}{E_2\pi}. \tag{4}$$

Here E_1, E_2 are the Young's moduli of elasticity for the obstacle surface and the damper colliding surface; ν_1 and ν_2 are their Poisson's coefficients.

The motion equations have the following form:

$$\begin{aligned} m_1\ddot{x}_1 + c_1\dot{x}_1 + k_1x_1 - c_2(\dot{x}_2 - \dot{x}_1) - k_2(x_2 - x_1 - V - C) \\ = F(t) - H(z)F_{con}(z), \\ m_2\ddot{x}_2 + c_2(\dot{x}_2 - \dot{x}_1) + k_2(x_2 - x_1 - V - C) = H(z)F_{con}(z). \end{aligned} \tag{5}$$

The initial conditions are:

$x_1(0) = 0,\ x_2(0) = V+C,\ \dot{x}_1(0) = \dot{x}_2(0) = 0.$

The Heaviside step function $H(z)$ "activates" the contact force $F_{con}(z)$ that acts only during an impact. The stiff set of differential equations of motion (5) is integrated using the stiff solver *ode23s* from the *Octave* platform.

 doi:10.20944/preprints202604.0099.v1

To implement the energy approach to assessing the damper efficiency, the total mechanical energy of the PS and the damper can be calculated after integrating the motion equations.

$$E_{1total}(t) = E_{1kinetic}(t) + E_{1poten}(t) = \frac{m_1\dot{x}_1(t)^2 + k_1x_1(t)^2}{2}$$
$$E_{2total}(t) = E_{2kinetic}(t) + E_{2poten}(t) = \frac{m_2\dot{x}_2(t)^2 + k_2\left(x_2(t) - (V + C)\right)^2}{2} \quad (6)$$

The following were adopted as basis structural parameters: m_1= 1000 kg, k_1=°3.95·10⁴ N/m, c_1= 452 N·s/m, E_1=°2.1·10¹¹ N/m², E_2= 2.05·10⁷ N/m², ν_1= 0.3, ν_2= 0.4, P= 800 N. The damper mass is m_2= 60 kg that is 6% of PS mass m_1. It is worth noting the value of Young's modulus for damper colliding surface E_2. Its value was determined in our previous work [30] by conducting an optimization procedure. It matches the softer material and provides a softer impact.

When performing the optimization procedures, the maximum PS energy E_1 is chosen as the objective function, which is calculated for P=800 N at the exciting force frequency ω=6.28 rad/s.

3. System Dynamics and Efficiency of the Dampers with Various Parameter Sets

3.1. The Dynamic Behavior of the System with 6 Different Dampers

By selecting the damper parameters for SSul NES (Figure 1d) as previously set for SSbl NES (Figure 1a) with a mass m_2=60 kg [31], and changing only the clearance C and distance V, we consider two damper parameter sets – Set 1 and Set 2. Then, the *surf* and *fminsearch* program from *Matlab* platform were used to find the optimized damper parameters. The optimization process using these programs was described in detail in our previous works [32,36]. The optimization process allowed us to select four more different sets of parameters: Sets 3, 4, 5, 6. These sets are presented in Table 1.

Table 1. The parameter Sets for SSul NES coupled with PS.

	k_2, N/m	c_2, N·s/m	C, m	V, m
Set 1	215	232	0.03	0.03
Set 2	215	232	0.05	0.1
Set 3	700.0	50.00	0.06000	0.1
Set 4	753.1	50.09	0.08286	0.1
Set 5	784.9	50.00	0.09975	0.1
Set 6	668.9	50.83	0.06233	0.1

The reduction in maximum mechanical PS energy E_{1max} resulting from the installation of these SSul NESs is shown in Figure 2.

 doi:10.20944/preprints202604.0099.v1

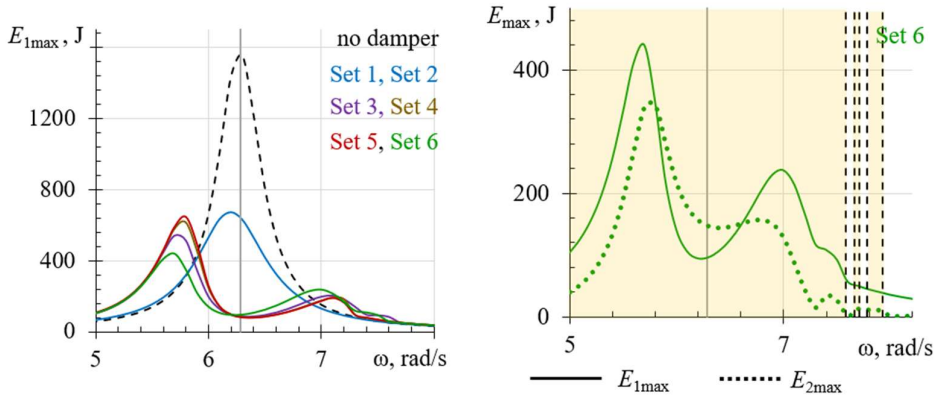

(**a**) (**b**)

Figure 2. (**a**) Reduction in maximum mechanical energy of the PS E_{1ma} through the use of six different SSul NESs. (**b**) Maximum energy of PS connected to SSul NES with parameter Set 6 and its energy shown by the dotted curve.

The curves for Set 1 and Set 2 merge in Figure 2a. The reduction in PS vibrations achieved by installation any of the other four dampers is similar. This graph once again confirms the thesis that there is a lot of damper parameter sets that provide similar efficiency in mitigating the PS vibrations. We selected a damper with Set 6 of the parameters for further consideration because its efficiency is slightly higher. The energy of PS coupled to this damper is shown separately in Figure 2b. The damper maximum energy E_{2max}, shown by the dotted curve is large due to its large displacements in the direction opposite to the obstacle, which are free and unlimited. The nonlinearity area in which the damper impacts occur is wide; it is shown in light yellow. The T-periodic motion with one impact per cycle occurs in this zone. However, at high frequency, the picture changes. The motions with different periodicities ($2T$, $3T$, $4T$) and different numbers of impacts per cycle (1, 2, and 3 impacts) alternate with irregular modes (chaotic and transient chaos) in the high - frequency range. In addition, there are narrow areas where movement occurs without impacts; these are shown in white and are bounded by vertical dashed lines. This rich and complex dynamics will be shown in detail below. The solid black vertical line indicates the resonant frequency.

3.2. Comparison with TMD and SSbl NES

The TMD tuning that determines its optimal parameters was carried out in [31]. Table 2 shows the optimal parameter values for SSul NES with Set 6, TMD, and SSbl NES for clarity and ease of comparison. Figure 3 demonstrates the reduction in the PS maximum energy due to the attachment of these dampers. The dotted curves present the maximum energy of the damper.

Table 2. The parameters of the dampers coupled with PS.

	k_2, N/m	**c_2, N·s/m**	**C, m**	**V or D, m**
SSul NES (Set 6)	669	50.8	0.062	V=0.1
TMD	600	262	–	–
SSbl NES	215	232	0.36	D=0.06

 doi:10.20944/preprints202604.0099.v1

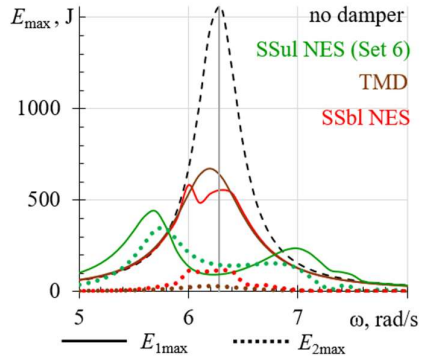

Figure 3. Reduction in maximum mechanical energy of the PS E_{1max} through the use of three different dampers.

Graph in Figure 3 shows that SSul NES with free movement away from the obstacle and unilateral impacts on the obstacle provides the greatest efficiency in mitigating the PS vibrations. Thanks to its large free displacements, it receives a large energy E_{2max} caused by energy transfer from PS, which allows for a significant reduction in PS energy. The efficiency of the SSbl NES and TMD is also quite high, but slightly lower. The energy transfer from PS is also best achieved with SSul NES, as this damper receives the highest energy E_{2max}.

4. Retention of the Tuning for Different Damper Types When Changing the Structural Parameters

Retention of the tuning clearly demonstrates the damper efficiency when changing the structural parameter over a wide range, if the tuning was made at its specific value. Such a study of changes in several structure parameters for a system with an attached SSbl NES was presented in detail in [31,36]. In this Section, such results are shown for a system with SSul NES coupled with PS for several structure parameters, namely for the PS natural frequency, which is characterized by its stiffness k_1, for its damping c_1, and for the intencity of the exciting force, which is characterized by its amplitude P. Retention of the SSul NES tuning is compared with that of TMD and SSbl NES.

4.1. Changing the Primary Structure Stiffness k_1

Changing the primary structure stiffness k_1 at a fixed mass changes its natural frequency, which is determined by the well-known formula $\omega_0 = \sqrt{k_1/m_1}$. If the optimal damper parameters have been determined for a specific stiffness value k_1, then when this value changes, the selected optimal parameters cease to be optimal, and the damper efficiency worsens. Figure 4 demonstrates the reduction in the PS maximum energy when its stiffness is changed for PS coupled with one of three dampers.

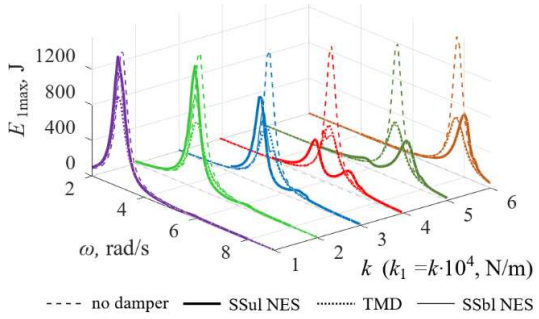

Figure 4. Reduction in maximum PS energy with attached SSul NES, TMD, and SSbl NES tuned to k_1=3.95·10^4 N/m when changing the PS stiffness k_1.

 doi:10.20944/preprints202604.0099.v1

The maximum PS energy has different behavior when its stiffness is increased or decreased. The tuning made for k_1=3.95·10⁴ N/m that is shown in Figure 4 in red worsens when this stiffness changes. Increasing stiffness deteriorates its reduction significantly less than decreasing it. The efficiency of all three damper types changes insignificantly and similarly as k_1 increases. However, when k_1 decreases the efficiency of all three dampers deteriorates strongly and quickly. The efficiency of SSul NES worsens the most, while TMD deteriorates the least. This is clearly visible in Figure 5.

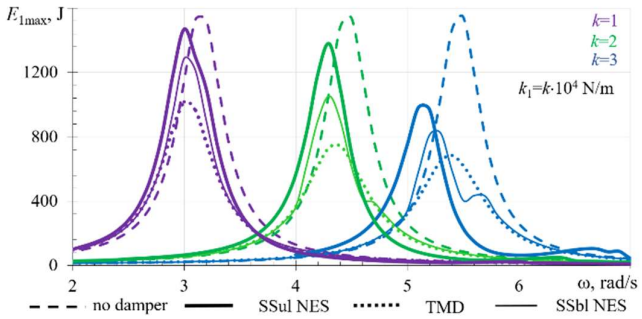

Figure 5. Reduction in maximum PS energy with attached SSul NES, TMD, and SSbl NES tuned to k_1=3.95·10⁴ N/m when decreasing the PS stiffness k_1.

Thus, increasing the PS stiffness, that is, its natural frequency, has a negligible effect on the efficiency of dampers that were tuned to a lower stiffness k_1 when the system is subjected to harmonic excitation. Reducing PS stiffness significantly impairs damper tuning and reduces their efficiency. TMD retains its tuning better than the other two.

4.2. Changing the Primary Structure Damping c_1

Changing the PS damping c_1 has a negligible effect on the damper efficiency. Figure 6 demonstrates the relationship between PS energy, which it has when operating without a damper and in combination with one of three different dampers. All dampers were tuned to PS damping c_1=452 N·s/m, which is shown in the middle graph, i.e., in Figure°6b. Both when increasing and decreasing c_1 the reduction in PS energy remains high and similar on all three graphs. SSul NES, that is, a single-sided vibro-impact damper with freely movement away from the obstacle, exhibits the best result in mitigating the PS vibrations.

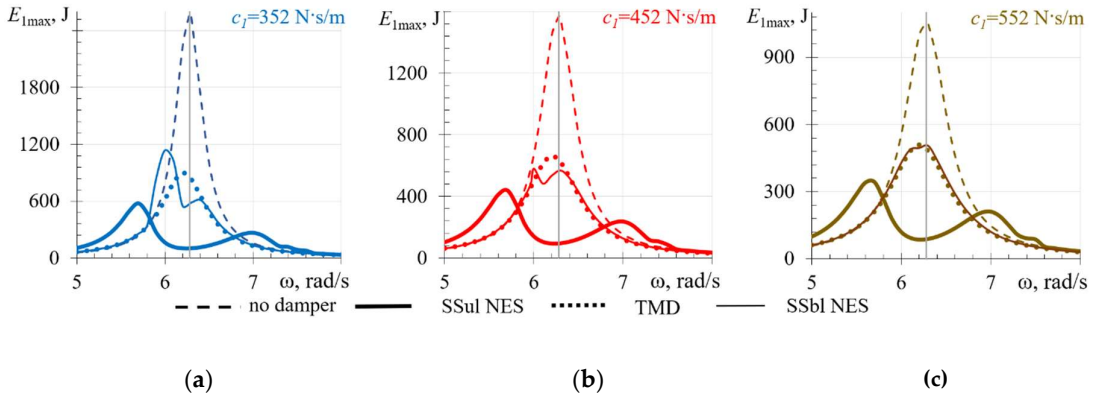

Figure 6. Reduction in maximum PS energy with attached SSul NES, TMD, and SSbl NES tuned to (**b**) c_1=452 N·s/m when (**a**) decreasing c_1=352 N·s/m and (**c**) increasing the PS damping c_1=552°N·s/m.

 doi:10.20944/preprints202604.0099.v1

4.3. Changing the Intensity of the External Load P

The system dynamic behavior when the amplitude of the exciting force P changes is similar to the behavior when the PS damping c_1 changes, which is clearly shown in Figure 7. Both when increasing and decreasing P the reduction in PS energy remains high and similar on all three graphs. SSul NES demonstrates the best result in mitigating the PS vibrations. It is necessary to note that the middle graph in red showing the basis tuning for k_1=3.95·10⁴ N/m, c_1=452 N·s/m, and P=800 N is repeated in several Figures for easer observation of the changes taking place.

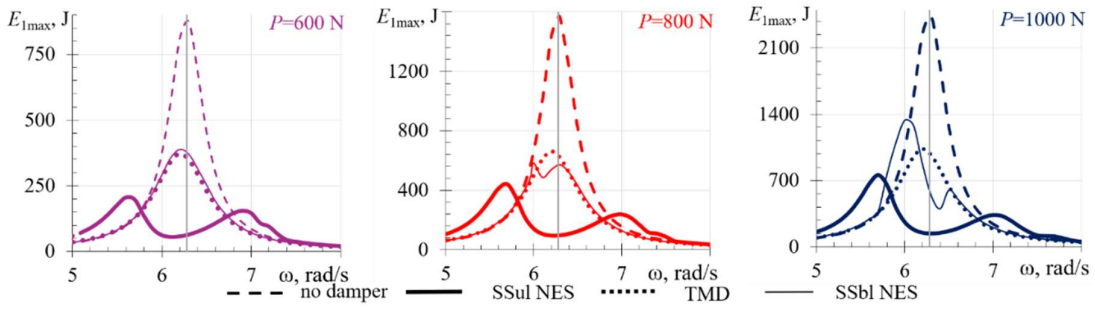

Figure 7. Reduction in maximum PS energy with attached SSul NES, TMD, and SSbl NES tuned to (**b**) P=800 N when (**a**) decreasing P=600 N and (**c**) increasing P=1000 N.

Thus, changing the PS damping c_1 and the intensity of the exciting force P does not cause significant changes in the damper dynamics and efficiency and allows the advantage of SSul NES to be demonstrated.

5. Dynamic Behavior of the System with SSul NES at Different Exciting Force Frequencies

The SSul NES with free movement away from the obstacle coupled with PS demonstrates quite calm dynamics while the SSbl NES exhibits rich complex dynamics [30,36]. The bifurcation diagram for SSul NES with parameters of Set 6 is presented in Figure 8. It is constructed using the basic values of structural parameters: k_1=3.95·10⁴ N/m, c_1=452°N·s/m, P=800 N. For clarity, the curve of PS maximum energy is shown conditionally and is displayed in green. The very wide area of T-periodic motion with one impact per cycle, designated as T,1, covers almost the entire frequency range. Only high frequencies cause its change and ensure the implementation of complex dynamics. Here, periodic motions with different periodicity (2T, 3T, and 4T) and different numbers of impacts per cycle quickly follow one another and alternate with irregular movements and regions of movement without impacts.

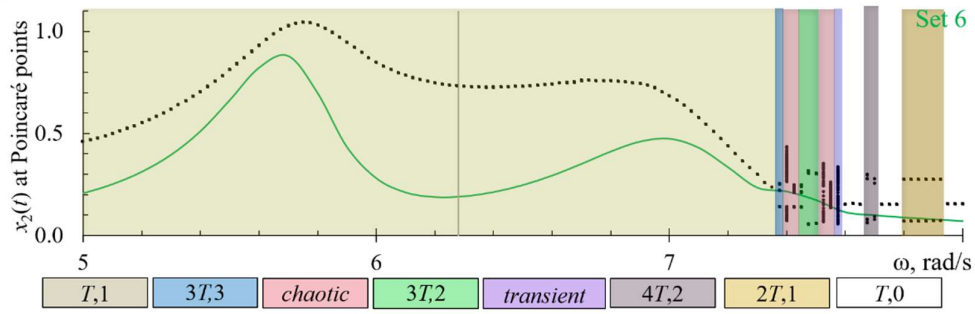

Figure 8. Bifurcation diagram for SSul NES with optimized parameters in Set 6.

 doi:10.20944/preprints202604.0099.v1

Let's look at several interesting regimes. Regime $3T,3$, i.e., the mode of $3T$ periodicity with 3 impacts per cycle occurs in the system at the exciting force frequency ω=7.375 rad/s. Figure 9 demonstrates its typical characteristics.

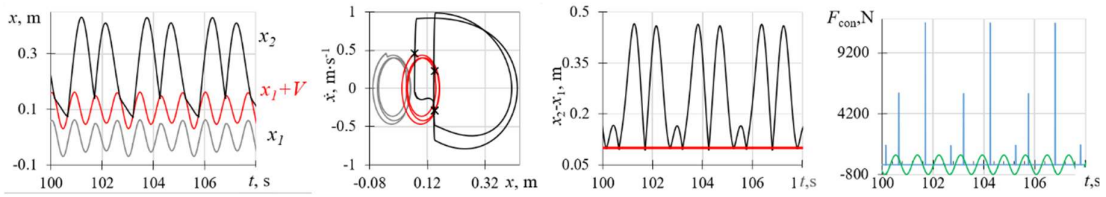

(**a**) (**b**) (**c**) (**d**)

Figure 9. Characteristics of $3T,3$ regime which occur in the system with SSul NES (Set 6) at exciting force frequency ω =7.375 rad/s. (**a**) Time histories of displacements of PS (gray), damper (black), and obstacle (red). (**b**) Phase trajectories of PS (gray), damper (black), and obstacle (red). (**c**) Relative displacements of the PS and damper $(x_2 - x_1)$ in black and obstacle $(x_2 - x_1 = V = 0.1$ m) in red. (**d**) The contact forces and the harmonic exciting force.

The displacement graph in Figure 9a clearly shows three damper impacts against the obstacle per cycle. Figures 9b and 9c also clearly demonstrate these three impacts per cycle, which generate different contact forces, as shown in Figure 9d.

The slightest change in the exciting force frequency causes chaotic behavior. The characteristics of the chaotic regime occurring at exciting force frequency ω=7.400 rad/s are shown in Figure 10.

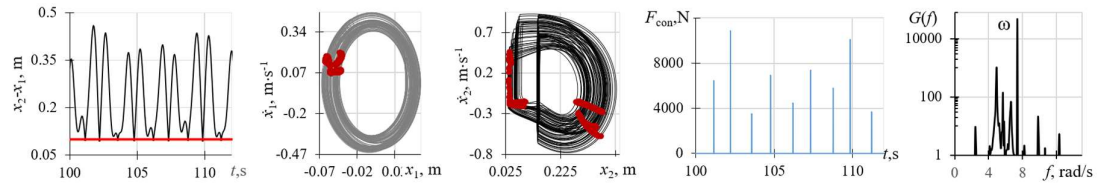

(**a**) (**b**) (**c**) (**d**) (**e**)

Figure 10. Characteristics of chaotic regime which occurs in the system with SSul NES (Set 6) at exciting force frequency ω=7.400 rad/s. (**a**) Relative displacements of the PS and damper $(x_2 - x_1)$ in black and obstacle $(x_2 - x_1 = V = 0.1$ m) in red. (**b**) Phase trajectories of PS with Poincaré map in red. (**c**) Phase trajectories of the damper with Poincaré map in red. (**d**) The contact forces. (**e**) Fourier spectrum.

The phase trajectories in the form of tangles, Poincaré maps in the form of smears, and a broad continuous Fourier spectrum are typical features of chaotic motion.

Transient chaos that occurs in the system at the exciting force frequency ω=7.575°rad/s exhibits an interesting phenomenon. The characteristics of this regime in both chaotic and periodic phases are shown in Figure 11. We emphasize that the transition from a chaotic phase to a periodic one occurs at the same exciting force frequency, which the transient chaos regime always demonstrates. The periodic phase is a T-periodic mode without any impacts, which is clearly visible in the contact force graph (Figure 11d) and phase trajectories with a single Poincaré map point (Figure 11f). It is worth paying attention to the low damper velocity values in the periodic phase. The compound motion of the damper consists of the translational motion together with PS and its relative motion with respect to PS. The absolute damper velocity $\dot{x}_2$ is the sum of the velocities in these two motions; in the periodic phase, it is shown in Figure 11g and is significantly lower than the PS velocity $\dot{x}_1$.

 doi:10.20944/preprints202604.0099.v1

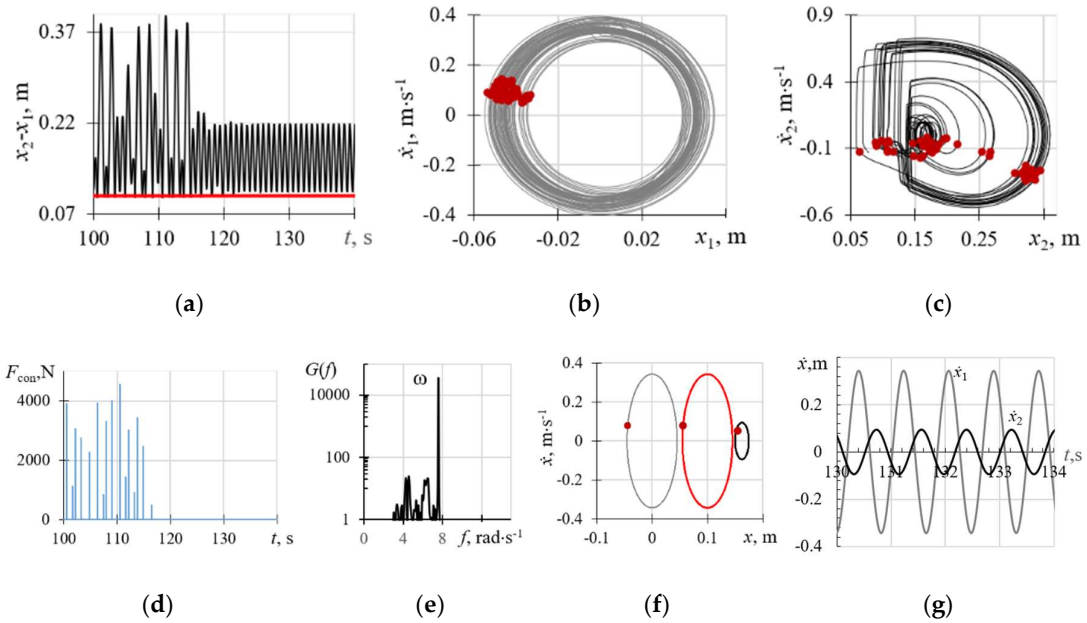

Figure 11. Characteristics of transient chaos which occurs in the system with SSul NES (Set 6) at exciting force frequency ω=7.575 rad/s. (**a**) Relative displacements of the PS and damper ($x_2 - x_1$) in black and obstacle ($x_2 - x_1 = V = 0.1$ m) in red. (**b**) Phase trajectories of PS with Poincaré map in red in chaotic phase. (**c**) Phase trajectories of the damper with Poincaré map in red in chaotic phase. (**d**) The contact forces. (**e**) Fourier spectrum. (**f**) Phase trajectories of the PS (gray), the obstacle (red), and the damper (black) with Poincaré maps in red in periodic phase. (**g**) Velocities of the PS (gray) and the damper (black) in periodic phase.

The behavior of PS and SSul NES energy in different motion regimes is shown in Figure 12.

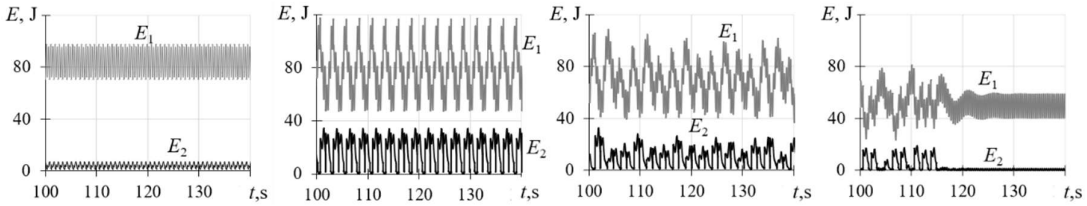

(**a**) Regime T,1 at ω=7.350 rad/s

(**b**) Regime 3T,3 at ω=7.375 rad/s

(**c**) Chaotic regime at ω=7.400 rad/s

(**d**) Transient chaos at ω=7.575 rad/s

Figure 12. The energy of PS E_1 and of SSul NES E_2 in different motion regimes.

6. Discussion

This study pays attention that performance, efficiency and dynamics of the SSVI NES are highly dependent on its design, more specifically, on the ability of the damper to move freely in the direction opposite the obstacle. From this point of view, there are four different SSVI NES designs. This paper examines in detail the performance and efficiency of one of them, namely the design that allows the damper to move freely away from the obstacle without any constraints, which in this paper is called SSul NES, that is, VI NES with unilateral impacts on the obstacle. Its dynamic behavior is compared with that for the TMD and SSVI NES with a design that allows not only impacts on the obstacle, but also the damper impacts on the PS directly, i.e. bilateral impacts, which in this paper is called SSbl NES. To evaluate the damping efficiency, an energy approach was chosen, that is, the reduction in the maximum PS energy was chosen as the damping efficiency criterion.

 doi:10.20944/preprints202604.0099.v1

The necessary optimization procedures are performed using *Matlab* platform tools; all damper parameters are optimized simultaneously. Previously conducted optimization has resulted in lower values of the Young's modulus of colliding damper surface, which ensures a softer damper impact on the obstacle. Optimization of the Young's moduli is possible due to simulation an impact in accordance with Hertz's quasi-static contact theory, which introduces these moduli into the formula for the contact interactive force. Optimization procedures provided the selection of several parameter sets for the damper with a mass ratio of 6%, which confirms the thesis that there is a lot of parameter sets that ensure similar damper efficiency. The dynamics of the SSul NES with one of these sets was examined in detail. Under harmonic excitation, it exhibited high efficiency, exceeding that of TMD and SSbl NES with optimized parameters; the curve of the maximum PS energy demonstrated two resonant peaks. The damper received a large amount of energy transferred from the PS due to its large free displacements in the direction opposite the obstacle. Retention of the damper tuning when changing the PS natural frequency, characterized by its stiffness at a fixed mass, differs when it increases and decreases. It changes insignificantly for all three damper types with increasing PS stiffness, but deteriorates significantly with its decrease. Moreover, for TMD it worsens less than for VI NESs; for SSul NES it worsens the most. The dynamics of the SSul NES, unlike that of SSBL NES, is calm with periodic motion with one impact per cycle across almost the entire frequency range. Only at high frequencies its dynamics becomes complex with alternating periodic regimes with different periodicities and different numbers of impacts per cycle as well as irregular modes such as chaotic and transient chaos.

In future work, it would be advisable to study the performance and efficiency of the SSVI NES with a design that does not allow the damper impacts on the PS directly, but allows some damper penetration into the PS. It is also necessary to study the dynamics and efficiency of SSVI NESs with different designs under transient loads, such as impulsive and blast ones.

7. Conclusions

This paper examines the influence of the SSVI NES movement in the direction opposite to the obstacle on its dynamics and efficiency in mitigating the vibrations of the PS subjected to the harmonic excitation. There are four SSVI NES models with different capabilities for moving away from the obstacle, only one of which allows free movement in this direction without any restrictions. This paper focuses specifically on this model, called SSul NES, because the damper performs unilateral impacts on the obstacle, unlike another model, called SSbl NES, which allowed for bilateral impacts on both the obstacle and the PS directly. The damper efficiency is assessed by the reduction of PS maximum mechanical energy. All damper parameters are optimized simultaneously. It has been shown that SSul NES with optimized parameters ensures the highest efficiency compared to SSbl NES and TMD. It has also been shown that the retention of tuning for these three damper types is similar when the structural parameters are changed. When the PS natural frequency, i.e., its stiffness at a fixed mass, changes, its increase insignificantly changes the damper tuning. On the contrary, its decreasing significantly worsens the tuning for all three damper types. The changes in the PS damping and in the exciting force intensity have negligible effect on damper tuning. The dynamics of SSVI NES with free motion away from the obstacle is quite calm with periodic motion over almost the entire frequency range. Rapid alternation of modes with different periodicity and different numbers of impacts per cycle, as well as irregular modes, is observed only at high frequencies of the exciting force. However, the presence of irregular regimes does not affect the damper efficiency.

 doi:10.20944/preprints202604.0099.v1

Author Contributions: Conceptualization, P.L. and O.P.; methodology, O.P.; software, T.P.; formal analysis, T.P.; investigation, O.P. and T.P.; writing—original draft preparation, O.P. and T.P.; writing—review and editing, O.P.; visualization, T.P.; project administration, P.L. All authors have read and agreed to the published version of the manuscript.

Funding: This research received no external funding.

Institutional Review Board Statement: Not applicable.

Informed Consent Statement: Not applicable.

Data Availability Statement: All the main data are contained in the article.

Conflicts of Interest: The authors declare no conflicts of interest.

References

1. Soto, M.G.; Adeli, H. Tuned mass dampers. *Arch. Comput. Methods Eng.* **2013**, *20*, 419–431. https://doi.org/10.1007/s11831-013-9091-7
2. Su, N.; Bian, J.; Peng, S.; Chen, Z.; Xia, Y. Balancing static and dynamic performances of TMD with negative stiffness. *Int. J. Mech. Sci.* **2023**, *243*, 108068. https://doi.org/10.1016/j.ijmecsci.2022.108068.
3. Love, J.S.; Haskett, T.C.; Morava, B. Effectiveness of dynamic vibration absorbers implemented in tall buildings. *Eng. Struct.* ***2018****, 176, 776–784. https://doi.org/10.1016/j.engstruct.2018.09.050.*
4. Love, J.S.; Morava, B. Practical experience with full-scale performance verification of dynamic vibration absorbers installed in tall buildings. *Int. J. High-Rise Build.* **2021**, *10*, 85–92. https://doi.org/10.21022/IJHRB.2021.10.2.85
5. Habib, G.; Kerschen, G. A principle of similarity for nonlinear vibration absorbers. *Physica D* **2016**, *332*, 1–8. https://doi.org/10.1016/j.physd.2016.06.001.
6. Jiang, X.; Lu, Z.-R.; Lin, X.; Yuan, J.; Wang, L.; Yang, D. An event-driven time-domain sensitivity method for optimizing parameters of vibro-impact NES cells to suppress multi-mode vibration. *J. Sound Vib.* **2026**, *628*, 119664. https://doi.org/10.1016/j.jsv.2026.119664
7. Chen, P.; Yang, J.-H.; Guo, X.-Y.; Liu, H.-T.; Yang, X.-D. Vibration analysis and vibration reduction strategy for an axially moving beam with a bistable nonlinear energy sinks. *Eur. J. Mech. A Solids* **2026**, *117*, 106029. https://doi.org/10.1016/j.euromechsol.2026.106029.
8. He, D.; Yang, N.; Liu, Y.; Xu, H.; Li, G.; Duan, Z.; Wang, T. Nonlinear vibration and vibration transmission of roll controlled by negative stiffness vibration absorbers. *Mech. Syst. Signal Process.* **2026**, *245*, 113872. https://doi.org/10.1016/j.ymssp.2026.113872.
9. Li, J.; Qiao, H.; Zeng, Z.; Huang, P. Wind vibration control in high-rise buildings using pre-tensioned nonlinear energy sink: Experimental and numerical study. *J. Build. Eng.* **2026**, *120*, 115488. https://doi.org/10.1016/j.jobe.2026.115488.
10. Li, H.; Ding, H.; Chang, T.; Chen, L. Optimization and performance analysis of a track tristable nonlinear energy sink subjected to impulsive, harmonic and sea wave excitations. *Appl. Ocean Res.* **2025**, *154*, 104404. https://doi.org/10.1016/j.apor.2024.104404.
11. Chen, L.; Liao, X.; Yin, L.; Ji, A.; Yan, J. Analytical study on periodic and quasi-periodic dynamics of vari-potential bi-stable nonlinear energy sink. *Preprints* **2026**. https://doi.org/10.21203/rs.3.rs-8616903/v1.
12. Di Egidio, A.; Contento, A. Enhancing seismic response in frame structures through rigid connections to structures with vibro-impacting mass. *Appl. Sci.* **2024**, *14*, 695. https://doi.org/10.3390/app14020695.
13. Abdollahi, A. Optimization and dynamic analysis of a vibro-impact nonlinear energy sink with electromagnetic coil for vibration suppression and energy harvesting. *Preprints* **2024**. https://doi.org/10.48550/arXiv.2411.17706.
14. Zeng, Y.-C.; Ding, H.; Ji, J.-C.; Chen, L.-Q. Theoretical and experimental study of a stable state adjustable nonlinear energy sink. *Mech. Syst. Signal Process.* **2024**, *216*, 111470. https://doi.org/10.1016/j.ymssp.2024.111470.

 doi:10.20944/preprints202604.0099.v1

15. Chen, Y.; Chen, N.; Ying, M. Research on target energy transfer and energy dissipation of coupled fractional-order inerter-based nonlinear energy sinks vibration system. *Fractal Fract.* **2026**, *10*, 104. https://doi.org/10.3390/fractalfract10020104.
16. Abdollahi, A.; Malekzadeh, M. Enhancing vibration control: A parallel integration of tuned mass damper with inerter and vibro-impact nonlinear energy sink. *Chaos Solitons Fractals* **2026**, *203*, 117658. https://doi.org/10.1016/j.chaos.2025.117658.
17. Zhao, H.; Li, J.; Sun, R.; Wang, S. Research on the dynamics and damping performance of parallel nonlinear energy sink cells. *J. Phys.: Conf. Ser.* **2025**, *3145*, 012033. https://doi.org/10.1088/1742-6596/3145/1/012033.
18. Nie, X.; Yang, M.; Lin, T.; Lou, J.; Lin, X.; Fu, J.; Yan, Z.; Wang, L. Frequency island effect and the vibration suppression performance of a bistable nonlinear energy sink–piezoelectric system coupled with the main structure. *Structures* **2026**, *85*, 111240. https://doi.org/10.1016/j.istruc.2026.111240.
19. Dekemele, K.; Habib, G.; Loccufier, M. The periodically extended stiffness nonlinear energy sink. *Mech. Syst. Signal Process.* **2022**, *169*, 108706. https://doi.org/10.1016/j.ymssp.2021.108706.
20. Dekemele, K.; Habib, G. Softening versus hardening nonlinear energy sinks: Forced vibration control and isolated resonance curves. *Nonlinear Dyn.* **2025**, *113*, 19179–19198. https://doi.org/10.1007/s11071-025-11164-6.
21. Li, W.; Wierschem, N.E.; Li, X.; Yang, T.; Brennan, M.J. Numerical study of a symmetric single-sided vibro-impact nonlinear energy sink for rapid response reduction of a cantilever beam. *Nonlinear Dyn.* **2020**, *100*, 951–971. https://doi.org/10.1007/s11071-020-05571-0.
22. Li, W.; Wang, Z.; Brennan, M.J.; Yang, T. Design and optimization of a two-degrees-of-freedom single-sided vibro-impact nonlinear energy sink for transient vibration suppression of a thin plate. *J. Sound Vib.* **2024**, *587*, 118512. https://doi.org/10.1016/j.jsv.2024.118512.
23. Weidemann, T.; Bergman, L.A.; Vakakis, A.F.; Krack, M. Energy transfer and localization in a forced cyclic chain of oscillators with vibro-impact nonlinear energy sinks. *Nonlinear Dyn.* **2025**, *113*, 14319–14360. https://doi.org/10.1007/s11071-025-10928-4.
24. Zhang, B.; Zhang, Z.; Jiang, J.; Zhang, Y.; Li, B.; Li, H.; Xian, H. Advantages of vibro-impact nonlinear energy sinks for vibration suppression of continuous systems: Coexistence of inter-modal energy scattering and targeted energy transfer. *Commun. Nonlinear Sci. Numer. Simul.* **2025**, *151*, 108993. https://doi.org/10.1016/j.cnsns.2025.108993.
25. Ledezma-Ramírez, D.F.; Rustighi, E.; Tapia González, P.E. Theoretical design and experimental validation of a vibro-impact support for vibration suppression. *Machines* **2026**, *14*, 206. https://doi.org/10.3390/machines14020206.
26. Di Egidio, A.; Briseghella, B.; Contento, A. Combined tuned mass damper and vibro-impacting nonlinear energy sink for the seismic protection of frame structures. *Structures* **2024**, *70*, 107576. https://doi.org/10.1016/j.istruc.2024.107576.
27. Abdollahi, A.; Malekzadeh, M. Synergistic damping: Optimizing vibration control with TMDI and VI-NES integration in nonlinear systems. *SSRN Preprints* **2024**. https://doi.org/10.2139/ssrn.4906091.
28. Wang, G.-X.; Ding, H.; Chen, L.-Q. Performance evaluation and design criterion of a nonlinear energy sink. *Mech. Syst. Signal Process.* **2022**, *169*, 108770. https://doi.org/10.1016/j.ymssp.2021.108770.
29. Lizunov, P.; Pogorelova, O.; Postnikova, T. Comparison of the performance and dynamics of the asymmetric single-sided and symmetric double-sided vibro-impact nonlinear energy sinks with optimized designs. *Int. J. Mech. Syst. Dyn.* **2024**, *4*, 303–316. https://doi.org/10.1002/msd2.12126.
30. Lizunov, P.; Pogorelova, O.; Postnikova, T. Features of different variants for optimal design of vibro-impact nonlinear energy sinks affecting their efficiency and dynamics. *Int. J. Nonlinear Mech.* **2025**, *179*, 105220. https://doi.org/10.1016/j.ijnonlinmec.2025.105220.
31. Lizunov, P.; Pogorelova, O.; Postnikova, T. Tuning of vibro-impact nonlinear energy sinks under changing structural parameters. Part 2. Comparison with tuned mass dampers. *Strength Mater. Theory Struct.* **2025**, *115*, 13–32. https://doi.org/10.32347/2410-2547.2025.115.13-32.
32. Lizunov, P.; Pogorelova, O.; Postnikova, T. Comparative analysis of the use of MATLAB tools for optimizing parameters with constraints. *Strength Mater. Theory Struct.* **2026**, *116*, in press.

 doi:10.20944/preprints202604.0099.v1

33. Li, J.; Li, S.-B.; Yu, G.-L.; Zhu, L. A single-sided vibro-impact bistable nonlinear energy sink designed for pulse and seismic control. *Structures* **2025**, *71*, 107958. https://doi.org/10.1016/j.istruc.2024.107958.
34. Li, J.; Sun, B.-X.; Yu, G.-L. Vibration mitigation for high-rise buildings by a single-sided vibro-impact bistable nonlinear energy sink. *Soil Dyn. Earthq. Eng.* **2026**, *203*, 110083. https://doi.org/10.1016/j.soildyn.2025.110083.
35. Goldsmith, W. *The Theory and Physical Behaviour of Colliding Solids*; Edward Arnold Publishers Ltd.: London, UK, 1960
36. Lizunov, P.; Pogorelova, O.; Postnikova, T. Retention of tuning for vibro-impact and linear dampers under periodic excitation. In *Proceedings of the 6th International Electronic Conference on Applied Sciences (ASEC 2025)*, Online, 3–7 February 2025; MDPI: Basel, Switzerland, 2026; p. 12. https://doi.org/10.3390/engproc2026124012.